

Sub-milliKelvin spatial thermometry of a single Doppler cooled ion in a Paul trap

S. Knüinz,¹ M. Herrmann,¹ V. Batteiger,¹ G. Saathoff,¹ T. W. Hänsch,¹ and Th. Udem¹

¹*Max-Planck-Institut für Quantenoptik, 85748 Garching, Germany*

(Dated: November 17, 2018)

We report on observations of thermal motion of a single, Doppler-cooled ion along the axis of a linear radio-frequency quadrupole trap. We show that for a harmonic potential the thermal occupation of energy levels leads to Gaussian distribution of the ion's axial position. The dependence of the spatial thermal spread on the trap potential is used for precise calibration of our imaging system's point spread function and sub-milliKelvin thermometry. We employ this technique to investigate the laser detuning dependence of the Doppler temperature.

PACS numbers: 37.10.Vz, 37.10.Rs, 37.10.Ty

I. INTRODUCTION

In the final stages of laser cooling the motion of an atom is dominated by the random recoils of photon absorption and emission events [1, 2]. If the atom is harmonically confined, this Brownian motion [3, 4] is expected to result in a Gaussian distribution of its position and velocity [5–7]. The width of this distribution can be intuitively interpreted as temperature, which we define as the time averaged energy divided by Boltzmann's constant for a single particle. This is a powerful notion, since many experiments require low residual kinetic energy, e.g., for precision metrology [8–12] or quantum computation and simulation [13, 14]. In this article we study the spatial probability density of a Doppler cooled Mg^+ ion trapped in a linear radio frequency (rf) trap, confirm the expected Gaussian distribution, and demonstrate that our straightforward imaging approach enables precise thermometry, as required for a wide range of experiments.

While in the strong-binding limit the comparison of the strengths of motional sidebands allows precise temperature measurements [15, 16], in the weak-binding limit the sidebands are not resolved. In this regime, ion temperatures are usually derived from the fluorescence line shapes which are decomposed into their Lorentzian lifetime contribution and the thermal distribution [17] by fitting a Voigt function. However, this method relies on the assumption of a Gaussian thermal distribution and the separation of the lifetime and thermal widths can be accompanied by rather large uncertainties [9, 18]. Upper limits for the temperatures of cooled ions have also been obtained by measuring the (thermal) spatial distribution in early laser cooling experiments [19]. Uncertainties down to 5 mK have recently been reported [20] by means of a specifically designed Fresnel lens with high spatial resolution. A similar technique has also been applied to atoms [21]. Thermometry on large ion crystals has been performed by comparing crystal images to the results of molecular dynamics simulations [22, 23].

In this work (see also [24]), we investigate the time-averaged spatial distribution of a single Mg^+ ion confined in a linear quadrupole trap and laser-cooled close to the

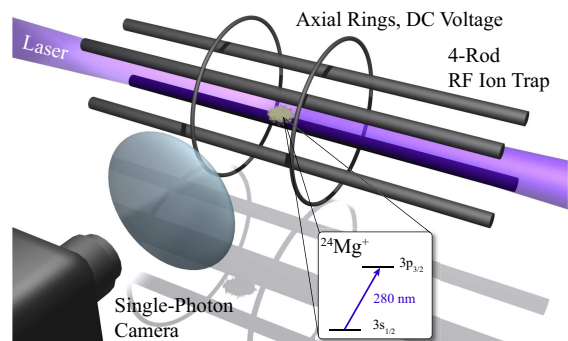


FIG. 1: (Color online) Experimental setup: A $^{24}\text{Mg}^+$ ion is trapped in a linear Paul trap. Radial confinement is accomplished by an rf voltage applied to two of the four rods. A dc voltage applied to the rings provides tunable axial confinement. The ion is Doppler cooled by red-detuned laser light addressing the cycling D_2 transition. A single-photon camera observes the axial spatial fluorescence distribution via an imaging system.

Doppler limit. The trap is operated with weak axial dc confinement which results in an axial spatial spread considerably larger than the resolution of our imaging optics. As expected for Doppler cooling, we observe a Gaussian fluorescence distribution. By accurately calibrating both the magnification and the resolution of our imaging optics, we are able to measure accurate values of the thermal spread which allow to extract ion temperatures with sub-mK uncertainties. We employ this precise thermometry to investigate the laser detuning dependence of the Doppler temperature.

II. THEORETICAL BACKGROUND

We consider an ion of mass m , trapped along the z -axis in a harmonic potential $V = m\omega^2 z^2/2$ with secular frequency ω , leading to motional quantum mechanical oscillator states $\psi_n(z)$ of energy $E_n = (n + 1/2)\hbar\omega$. Under the assumption that the ion's random walk caused by the stochastic photon absorption and emission is ergodic, the single ion can be assigned a temperature T which quan-

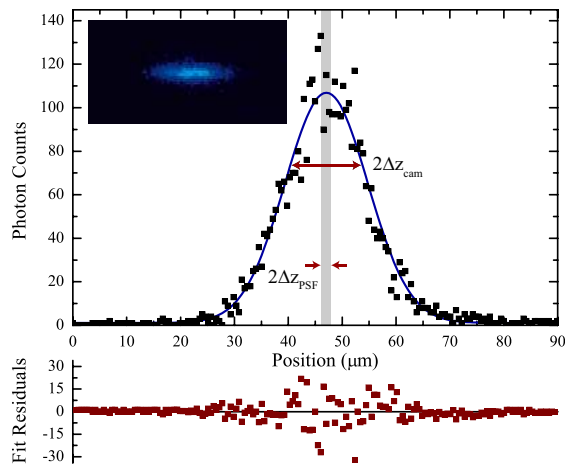


FIG. 2: (Color online) Time-averaged spatial distribution of a single laser-cooled ion trapped with secular frequency $\omega = 2\pi \times 15$ kHz ($T \approx 1$ mK). The inset shows the ion image while the plot is a histogram in axial direction. The residuals (lower graph) of a Gaussian fit (solid line) confirm a normal distribution as expected from Brownian motion caused by the recoils of stochastic photon scattering events. The RMS width Δz_{cam} of the Gaussian and the RMS resolution $\Delta z_{PSF} \approx 1 \mu\text{m}$ of our imaging system are indicated.

tifies the time-averaged occupation number of the states $\bar{n} = (\exp[\hbar\omega/k_bT] - 1)^{-1}$ [25] with the Boltzmann constant k_b . The population probabilities P_n of the states $\psi_n(z)$ follow the distribution $P_n = \bar{n}^n (\bar{n} + 1)^{-(n+1)}$ [25] which translates into a time-averaged spatial distribution of the ion around its mean position z_0

$$f(z) = \sum_{n=0}^{\infty} P_n |\psi_n(z)|^2 = \frac{1}{\sqrt{2\pi}\Delta z_{th}} e^{-\frac{(z-z_0)^2}{2\Delta z_{th}^2}}. \quad (1)$$

In the evaluation of the sum we used Mehler's Hermite polynomial formula [26]. The variance of this Gaussian is $\Delta z_{th}^2 = (\bar{n} + 1/2)\hbar/(m\omega)$. For $k_bT \gg \hbar\omega$ as appropriate for the weak binding regime we have $\bar{n} \approx k_bT/(\hbar\omega)$ and the root mean square (RMS) width

$$\Delta z_{th} \approx \sqrt{\frac{k_bT}{m\omega^2}}. \quad (2)$$

The temperature limit of a Doppler-cooled ion due to secular motion in a harmonic potential results from an equilibrium of laser-induced cooling and heating rates and is given by [27]

$$T = \frac{\hbar\Gamma}{8k_b}(1 + \xi) \left((1 + s) \frac{\Gamma}{2|\Delta|} + \frac{2|\Delta|}{\Gamma} \right). \quad (3)$$

It depends on the laser detuning $\Delta < 0$ and the laser intensity $I = sI_{sat}$, where s and I_{sat} are the saturation parameter and intensity, respectively. Γ is the natural linewidth of the optical dipole transition and $\xi = 2/5$ takes the dipole emission pattern into account.

The temperature diverges for $|\Delta| \rightarrow 0$, $|\Delta| \rightarrow \infty$, and $s \rightarrow \infty$. The minimum of $T_{min} = \sqrt{1 + s(1 + \xi)}\hbar\Gamma/4k_b$ is obtained at a detuning of $\Delta_{min} = -\Gamma\sqrt{1 + s}/2$ which, for small s , reduces to $\Delta_{min} \approx -\Gamma/2$.

III. EXPERIMENTAL SETUP

Our experimental setup is shown in Fig. 1 (see also [11]). A single $^{24}\text{Mg}^+$ ion is trapped in a linear rf quadrupole trap which operates at a trap frequency $\Omega = 2\pi \times 22.6$ MHz and generates radial rf confinement with a secular frequency $\omega_r \approx 2\pi \times 1$ MHz. The trap electrodes are surrounded by two rings with a dc voltage applied to generate axial confinement tunable from $\omega \approx 2\pi \times 10$ to 150 kHz. These frequencies are measured by secular excitation with a weak external signal and can thus be controlled with an accuracy of $\Delta\omega < 2\pi \times 1$ kHz. Since $\omega_r \gg \omega$, axial and radial motion are decoupled so that we can neglect radial movement in the following. Due to its zero nuclear spin, the alkali-like spectrum of $^{24}\text{Mg}^+$ shows no hyperfine structure and the D_1 and D_2 lines constitute clean cycling transitions well suited for Doppler cooling without the need for repumper lasers. Two laser beams each stabilized in frequency and intensity address the $3^2S_{1/2} \rightarrow 3^2P_{3/2}$ D_2 transition near 280 nm (natural linewidth $\Gamma = 2\pi \times 41.8(4)$ MHz [28], $I_{sat} = 2.50$ kW/m 2). One beam is aligned along the axial trap direction. The second laser beam is slightly tilted by 14° against the first beam to provide radial cooling. The beams are detuned with respect to each other by ≈ 500 kHz to avoid a stable interference pattern. The ion is imaged with a $f/2$ condenser lens and a microscope objective onto a single-photon camera (SPC, Quantar Mepsicron II). Because of the SPC's limited spatial resolution of $56 \mu\text{m}$, a magnification of $M \approx 100$ is chosen for the imaging system. The detector plane is digitized in pixels of $49 \mu\text{m}$ size. The conversion factor between the real space object size in μm and image size in pixels is calibrated accurately by measuring the distance between two simultaneously trapped ions in the imaging plane of the camera for several trapping potentials ω [29]. The RMS resolution of the imaging system's point spread function (PSF) at 280 nm is $\Delta z_{PSF} \approx 1 \mu\text{m}$ for optimal alignment. It derives from the resolution of the lens system, the resolution of the camera, and the discretization of the camera data. However it is diminished when the ion is shifted out of focus, particularly by varying laser forces, and thus becomes slightly detuning dependent. After conversion into μm in object space, the RMS spot size Δz_{cam} of a recorded ion image appears as a convolution of the thermal spread Δz_{th} with the finite PSF width Δz_{PSF} . Assuming the PSF to be Gaussian, we have:

$$\Delta z_{cam} = \sqrt{\Delta z_{PSF}^2 + \Delta z_{th}^2}. \quad (4)$$

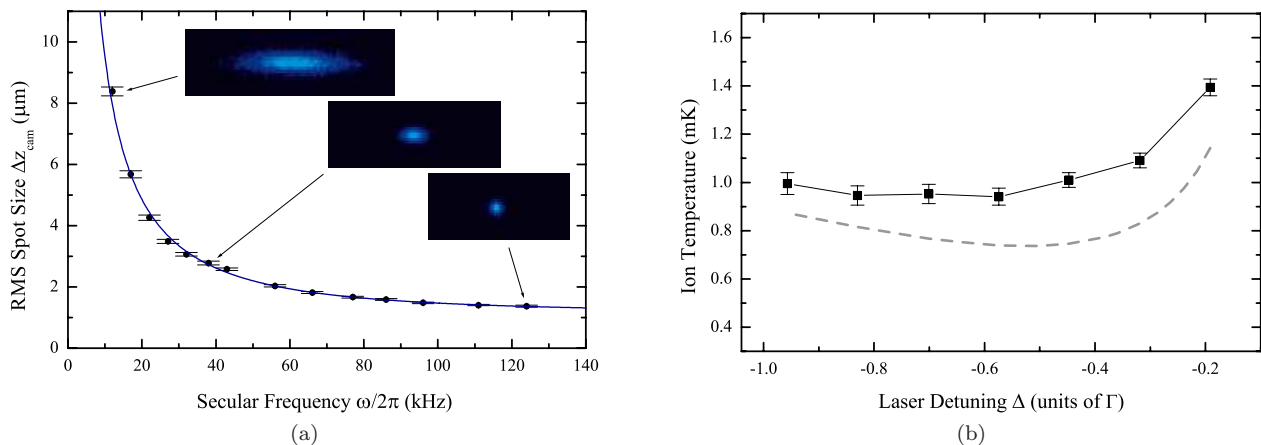


FIG. 3: (Color online) (a) Measurement of the spot size Δz_{cam} of the ion images with $\Delta = -2\pi \times 18.7$ MHz and $s \lesssim 0.1$ for various trapping potentials $\omega/2\pi$. The insets show exemplary ion images. From a fit (solid line) of Eqs. 2 and 4, we obtain an ion temperature of $T = 1.02(3)$ mK and a PSF of $\Delta z_{PSF} = 1.13(3)$ μm RMS with statistical uncertainties. (b) Same analysis for various laser detunings Δ . Results are shown as squares together with temperatures expected from Eq. 3 (dashed gray line). We attribute the observed temperature excess of up to ≈ 0.2 mK to systematic micromotion, see discussion in the text. The values of Δz_{PSF} obtained for all data points agree within their statistical uncertainties. This measurement demonstrates the precision of the thermal spread thermometry providing a total accuracy of < 0.3 mK unchallenged by other methods in the unresolved sideband regime.

IV. MEASUREMENT AND RESULTS

A. Time-averaged spatial distribution

The inset of Fig. 2 shows an image of a Mg^+ ion trapped with a secular frequency $\omega = 2\pi \times 15$ kHz and cooled close to the Doppler limit of about $T \approx 1$ mK ($\bar{n} \approx 1400$). From Eq. 2 follows a RMS spatial spread of $\Delta z_{th} \approx 8$ μm which is about eight times larger than the PSF of our imaging system. In this case, with Eq. 4, the PSF only contributes $\approx 1\%$ to the width Δz_{cam} of the image. The laser detuning is set to $\Delta = -2\pi \times 40$ MHz $\approx -\Gamma$, and the total laser intensity – with both laser intensities equal at the location of the ion – is limited to $s \lesssim 0.1$ which is monitored by the observed photon scattering rate. Figure 2 shows a histogram of the axial spatial distribution obtained from the image. No statistically significant deviation from a Gaussian could be found with a fit, as can be seen from the residuals, which confirms the stochastic nature of the ion’s motion. The RMS spot size of the ion image of $\Delta z_{cam} = 7.7(1)$ μm is indicated by the horizontal bar, while the vertical bar shows the resolution of our imaging system.

B. Spatial thermometry measurement

In order to obtain a precise value of the absolute temperature for larger oscillation frequencies ω as well, we need to determine Δz_{PSF} more accurately. We use the fact that, according to the laws of Brownian motion, the width Δz_{th} of the thermal distribution varies $\propto 1/\omega$

(Eq. 2). From measurements of the spot sizes Δz_{cam} for different ω , we obtain Δz_{PSF} , Δz_{th} , and thus the absolute temperature T of the ion from a fit of Eqs. 2 and 4. This method depends on the shape of the PSF and the constancy of its width Δz_{PSF} . The ion images at high secular frequencies which reflect the PSF do not show a significant deviation from a Gaussian. To ensure the constancy of its width, we readjust the imaging system for optimal resolution at each data point, thus compensating the effects of ion position changes due to the varying balance between the trap potentials and the laser force. At the same time we minimize radial micromotion at each data point to avoid axial heating via possible coupling to the radial motion. Figure 3 (a) shows such a measurement for $\Delta = -2\pi \times 18.7$ MHz and $s \lesssim 0.1$ with ω between $2\pi \times 12$ and 124 kHz. The insets show corresponding images and the resulting axial RMS spot sizes Δz_{cam} obtained from Gaussian fits to the image histograms are plotted versus $\omega/2\pi$. Note that the radial widths only increase slightly by about 15 % towards lower axial potentials because radial micromotion compensation becomes increasingly difficult. The $1/\omega$ behavior of Δz_{th} is confirmed by a fit (Eq. 4), which yields an ion temperature of $T = 1.02(3)$ mK and a PSF of $\Delta z_{PSF} = 1.13(3)$ μm , both with statistical uncertainties.

C. Systematic effects

The main systematic uncertainty arises from residual axial micromotion caused by the axial component of the rf fringe fields. The simultaneous presence of dc and rf fields leads to a parametric potential $V(t) =$

$\frac{1}{8}m\Omega^2(a - 2q\cos(\Omega t))z^2$. Ω is the trap frequency. $a \propto eU_{dc}/m\Omega^2$ and $q \propto eV_{rf}/m\Omega^2$ are trap parameters associated with the dc and rf voltages U_{dc} and V_{rf} , respectively. Without damping and diffusion, the ion's equation of motion is a Mathieu equation and for certain parameter sets (a, q) there are stable trajectories of the ion $z(t) = z_s \cos(\omega t)(1 + \frac{q}{2} \cos \Omega t)$ with amplitude z_s and $\omega \approx \frac{1}{2}\Omega(a + q^2/2)^{1/2}$ [30]. The latter can be interpreted as the secular frequency of the ion in a time averaged pseudopotential. For vanishing a it reduces to pure rf confinement $\omega_{rf} = q\Omega/\sqrt{8}$ while pure dc confinement $\omega_{dc} = \sqrt{a}\Omega/2$ results for $q = 0$. Superimposed on the secular motion, the ion performs micromotion at the trap frequency Ω with an amplitude $z_\mu = qz_s/2$. For an ion cooled close to the Doppler limit of 1 mK, z_μ is of the order of 50 nm and does not influence the apparent spread or lead to significant deviations from a Gaussian distribution [6, 31].

A stronger effect due to micromotion is expected via the kinetic energy which is given by [30]

$$E_{kin} = \frac{1}{4}m\omega^2 z_s^2 + \frac{1}{4}m\omega_{rf}^2 z_s^2 + \frac{1}{2}m\frac{\omega_{rf}^2 \omega_{dc}^2}{\omega^2} \Delta z_0^2. \quad (5)$$

The first term is due to secular motion, the second reflects the contribution from the unavoidable *ordinary* micromotion that is associated with the secular motion. It depends on the secular amplitude z_s and is significant for low secular frequencies $\omega \approx \omega_{rf}$. The third term is caused by a mismatch Δz_0 between the rf and dc potential minima positions. It results in a displacement $\delta z = \Delta z_0 \omega_{dc}/\omega$ of the ion out of the rf minimum so that it is exposed to *excess* micromotion [30] that contributes an energy $E_{kin}^{excess} = \frac{1}{2}m\omega_{rf}^2 \delta z^2$. A cooling laser introduces both damping and a stochastic force to the equation of motion. Blatt et al. [6] have solved the corresponding Fokker-Planck equation for the first two terms in eq. 5, which results in Gaussian spatial and velocity distributions. It turns out that the presence of a stochastic force transforms part of the micromotion energy into irregular motion (temperature) by rf heating which is reflected in a broadening of the velocity distribution as well as the spatial distribution as compared to the case of pure secular motion.

From the lowest secular frequency that we have observed when lowering the dc potential a , we estimate an upper limit for the residual axial rf confinement of $\omega_{rf} = 2\pi \times 7$ kHz, corresponding to $q = 8.8 \times 10^{-4}$. According to [6], the corresponding *ordinary* rf heating broadens the spatial distribution by a factor of 1.15 for the lowest secular frequency of $\omega = 2\pi \times 12$ kHz. This broadening decreases strongly towards higher $\omega \gg \omega_{rf}$. For the estimated upper limit of $\omega_{rf} = 2\pi \times 7$ kHz, our Eq. 2 thus overestimates the temperature by a factor of 1.3 which results in a systematic uncertainty of ≈ 0.3 mK in our experiment.

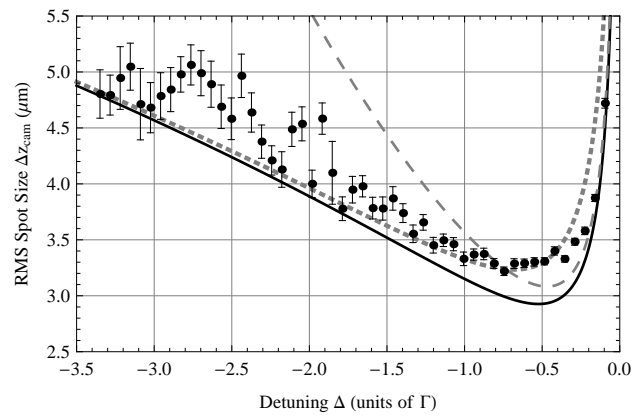


FIG. 4: Measured ion image spot size Δz_{cam} versus laser detuning for $s \approx 0.1$ and fixed $\omega = 2\pi \times 32$ kHz. The black solid line shows the result expected from Doppler cooling according to Eqs. 3, together with Eq. 2 and 4 using $s = 0.1$ and $\Delta z_{PSF} = 1.5 \mu\text{m}$. Qualitative agreement with the overall temperature behavior of Eq. 3 is found. However quantitatively the measured spreads and thus the temperatures are about 10% higher than expected which we attribute to rf heating due to excess micromotion, which depends on the photon scattering rate and thus decreases towards larger detunings. The gray long-dashed line represents Doppler cooling with an additional detuning-independent heating rate, the short-dashed line assumes a broadening of the line to 1.1Γ as caused, e.g., by magnetic fields. Both assumptions can not explain the observed thermal spread. Larger error bars for larger negative detunings are due to lower photon count rate.

D. Thermometry of a Doppler cooled ion

In the next step, we employ our thermometry method to investigate the detuning dependence of Doppler cooling. Figure 3 (b) shows absolute temperatures measured for laser detunings Δ between -0.2 and -1.0Γ indicated by squares while the circles are the Doppler temperatures predicted for pure secular motion by Eq. 3. Our measurements follow the detuning dependence of Eq. 3 qualitatively, but show an offset of ≈ 0.2 mK. The higher temperatures are on the order of our conservative estimate for the systematic uncertainty. However, such a temperature rise can also be caused by *excess* micromotion in a significantly smaller residual axial rf potential [30]. While the ordinary micromotion becomes insignificant for $\omega \gg \omega_{rf}$, excess micromotion due to a large $\Delta z_0 \gg z_s$ leads to a ω -independent contribution $E_{kin}^{excess} \approx \frac{1}{2}m\omega_{rf}^2 \Delta z_0^2$ in Eq. 5 and may thus increase the ion temperature through rf heating correspondingly.

In order to study the temperature over a wider range of detunings between 0 and -3.5Γ , we measure the image spot sizes Δz_{cam} of the ions for fixed values of $\omega = 2\pi \times 32$ kHz and $s \approx 0.1$ (Fig. 4). At this secular frequency the ordinary micromotion increases the ion temperature by less than 1%. Due to possible variations of the resolution Δz_{PSF} during the laser scan, we do not extract the temperature in this measurement.

Nevertheless, the spot size Δz_{cam} can still serve as a decent measure for the temperature. The solid line in Fig. 4 represents the behavior according to Eq. 3 in combination with Eqs. 2 and 4, using $s = 0.1$ and $\Delta z_{PSF} = 1.5 \mu\text{m}$. The latter is estimated to be an upper limit. Quantitatively, the measured values are again up to 10% higher. The data supports our hypotheses that rf heating due to excess micromotion is the main cause of the higher observed temperatures. Since rf heating is related to the photon scattering of the cooling laser [6], its rate is expected to be detuning-dependent similar to the cooling rate. The wide tuning range in this measurement allows to exclude two other possible effects as causes for the excess temperature. As a comparison, the long-dashed line shows the expected broadening taking an additional, detuning-independent heating rate into account. The short-dashed line assumes that the line width is homogeneously broadened to 1.1Γ caused, e. g., by the Zeeman splitting or micromotion-induced line broadening [30]. From earlier spectroscopy experiments [9], we know that for our experimental parameters the homogeneous broadening is in fact lower. In conclusion, both effects can be excluded as causes for

the observed higher thermal spreads (temperatures).

V. SUMMARY

To summarize, we have demonstrated that a single, Doppler cooled ion weakly bound in an ion trap, shows a Gaussian thermal spatial distribution as expected from Brownian motion. We show that this time-averaged spatial distribution can be used for sub-milliKelvin thermometry with an accuracy of $< 0.3 \text{ mK}$ unchallenged by similar methods in the unresolved sideband regime. Further, we have employed this thermometry to investigate the detuning dependence of the temperature in Doppler cooling. Note that this method which was demonstrated for the axial trapping direction here, can in principle be applied to any projection of an ion on the imaging plane. The use of high NA objectives with resolutions close to the diffraction limit [20, 32] would allow to further improve on accuracy and to perform thermometry in steeper trapping potentials.

-
- [1] D. J. Wineland and W. M. Itano, Phys. Rev. A, **20**, 1521 (1979).
 - [2] S. Stenholm, Rev. Mod. Phys., **58**, 699 (1986).
 - [3] R. Brown, Phil. Mag. **4**, 161–173 (1828).
 - [4] A. Einstein, Annalen der Physik **17**, 549–560 (1905).
 - [5] G. E. Uhlenbeck and L. S. Ornstein, Phys. Rev. **36**, 823, (1930).
 - [6] R. Blatt, P. Zoller, G. Holzmueller, and I. Siemers, Z. Phys D. **4**, 121-126 (1986).
 - [7] D. M. Meekhof, C. Monroe, B. E. King, W. M. Itano, and D. J. Wineland, Phys. Rev. Lett. **76**, 1796 (1996).
 - [8] C. W. Chou, D. B. Hume, J. C. J. Koelemeij, D. J. Wineland, and T. Rosenband, Phys. Rev. Lett., **104**, 070802 (2010).
 - [9] M. Herrmann, V. Batteiger, S. Knünz, G. Saathoff, Th. Udem and T.W. Hänsch, Phys. Rev. Lett. **102**, 013006 (2009).
 - [10] R. Maiwald, D. Leibfried, J. Britton, J. C. Bergquist, G. Leuchs, and D. J. Wineland, Nat. Phys., **5**, 551 (2009).
 - [11] S. Knünz, M. Herrmann, V. Batteiger, G. Saathoff, T.W. Hänsch, K. Vahala and Th. Udem, Phys. Rev. Lett. **105**, 013004 (2010).
 - [12] Shlomi Kotler, Nitzan Akerman, Yinnon Glickman, Anna Keselman, Roe Ozeri, Nature **473**, 61 (2011).
 - [13] A. Friedenauer, H. Schmitz, J. T. Glueckert, D. Porras, and T. Schaetz, Nat. Phys., **4**, 757–761 (2008).
 - [14] D. Kielpinski, C. Monroe, and D. J. Wineland, Nature, **417**, 709–711 (2002).
 - [15] J. C. Bergquist, Wayne M. Itano, and D. J. Wineland, Phys. Rev. A, **36**, 428 (1987).
 - [16] L. Slodička, G. Hétet, N. Röck, S. Gerber, P. Schindler, M. Kumph, M. Henrich, and R. Blatt, e-print arXiv:1202.4559v1.
 - [17] W. Nagourney, G. Janik, and H. Dehmelt, Proc. Natl. Acad. Sci. USA, **80**, 643-646 (1983).
 - [18] Taro Hasegawa, Daisuke Tanooka, and Tadao Shimizu, Phys. Rev. A, **58**, 2327 (1998).
 - [19] W. Neuhauser, M. Hohenstatt, and P. E. Toschek and H. Dehmelt, Phys. Rev. A, **22**, 1137 (1980).
 - [20] B.G. Norton, E.W. Streed, M.J. Petrasianus, A. Jechow, and D. Kielpinski, arXiv:1106.1708v1 (2011). N. J. Phys. **13**, 113022 (2011).
 - [21] Y. Miroshnychenko, D. Schrader, S. Kuhr, W. Alt, I. Dotsenko, M. Khudaverdyan, A. Rauschenbeutel, and D. Meschede, Opt. Express **11**, 3498-3502 (2003).
 - [22] M. Drewsen, C. Brodersen, L. Hornekaer, J. S. Hangst, and J. P. Schiffer, Phys. Rev. Lett. **81**, 2878 (1998).
 - [23] D. Offenberger, C. B. Zhang, Ch. Wellers, B. Roth, and S. Schiller, Phys. Rev. A, **78**, 061401(R) (2008).
 - [24] S. Knünz, PhD thesis, Ludwig-Maximilians-Universität, Munich, Germany (2011).
 - [25] F. Reif, *Fundamentals of Statistical and Thermal Physics* (McGraw-Hill, New York, 1965).
 - [26] G. N. Watson, J. London Math. Soc. **8**, 194 (1933).
 - [27] D. Leibfried, R. Blatt, C. Monroe, and D. Wineland, Rev. Mod. Phys., **75**, 281 (2003).
 - [28] W. Ansbacher, Y. Li, and E. H. Pinnington, Phys. Lett. A, **139**, 165 (1989).
 - [29] D. F. V. James, Appl. Phys. B, **66**, 181–190 (1998).
 - [30] D. J. Berkeland, J. D. Miller, J. C. Bergquist, W. M. Itano, and D. J. Wineland, J. of Appl. Phys., **83**, 5025 (1998).
 - [31] J.I. Cirac, L.J. Garay, R. Blatt, A. S. Parkins and P. Zoller, Phys. Rev. A **49**, 421 (1994).
 - [32] A. Jechow, E. W. Streed, B. G. Norton, M. J. Petrasianus, and D. Kielpinski, Opt. Lett., **36**, 1371 (2011).